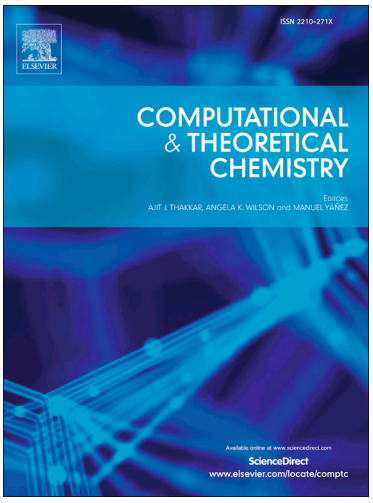

Density Functional Theory Studies of the Uncatalysed Gas-Phase Oxidative Dehydrogenation Conversion of *n*-Hexane to Hexenes

N.E. Damoyi, H.B. Friedrich, H.G. Kruger, D. Willock

PII: S2210-271X(17)30259-1
DOI: http://dx.doi.org/10.1016/j.comptc.2017.05.026
Reference: COMPTC 2521

To appear in: *Computational & Theoretical Chemistry*

Received Date: 22 March 2017
Revised Date: 19 May 2017
Accepted Date: 19 May 2017

Please cite this article as: N.E. Damoyi, H.B. Friedrich, H.G. Kruger, D. Willock, Density Functional Theory Studies of the Uncatalysed Gas-Phase Oxidative Dehydrogenation Conversion of *n*-Hexane to Hexenes, *Computational & Theoretical Chemistry* (2017), doi: http://dx.doi.org/10.1016/j.comptc.2017.05.026

Density Functional Theory Studies of the Uncatalysed Gas-Phase Oxidative Dehydrogenation Conversion of *n*-Hexane to Hexenes

N.E. Damoyi[a,*], H.B. Friedrich[b], H.G. Kruger[c] and D. Willock[d]

[a]Department of Chemistry, Mangosuthu University of Technology, Box 12363, Jacobs, 4026, South Africa, E-mail: damoyi@mut.ac.za

[b]School of Chemistry, University of KwaZulu Natal, Westville Campus, Private Bag X 54001, Durban, 4000, South Africa

[c]Catalysis and Peptide research unit, School of Pharmacy, University of KwaZulu Natal, Westville Campus, Private Bag X 54001, Durban, 4000, South Africa

[d]School of Chemistry, Cardiff University, Park Place, Cardiff CF10 3AT, Wales, UK

Keywords: DFT, ODH, *n*-hexane, RDS, mechanism.

ABSTRACT

Density Functional Theory (DFT) modelling studies were conducted for the activation of *n*-hexane in the gas-phase under experimental conditions of 573, 673 and 773K.

The aim of the study was to establish the most favourable radical mechanism for the oxidative dehydrogenation (ODH) of *n*-hexane to 1- and 2-hexene. Modelling of the 3-hexene pathway was omitted due to absence of this product in laboratory experiments. Computations were performed using GAUSSIAN 09W and molecular structures were drawn using the GaussView 5.0 graphics interface. The B3LYP hybrid functional and the 6-311+g(d,p) basis set were utilized for all the atoms. The most kinetically and thermodynamically favourable pathways are proposed based on the determination of the relative total energies ($\Delta E^{\#}$, ΔE, $\Delta G^{\#}$ and ΔG) for the different reaction pathways. The initial C-H activation step is β-H abstraction from *n*-hexane (C_6H_{14}) by molecular oxygen (O_2) to form the alkoxy ($C_6H_{13}O\cdot$) and hydroxyl ($\cdot OH$) radicals. This is proposed as the rate-determining step (RDS) with the calculated $\Delta E^{\#}$ = +42.4 kcal/mol. Two propagation pathways that involve, separately, the $C_6H_{13}O\cdot$ and $\cdot OH$ radicals may lead to the formation of 2-hexene. In both the propagation pathways, the $C_6H_{13}O\cdot$ and $\cdot OH$ radicals activate further C_6H_{14} molecules to produce $C_6H_{13}OH$ and H_2O, respectively, and the alkyl radicals ($\cdot C_6H_{13}$). Thereafter, one pathway involves the interaction of the $\cdot C_6H_{13}$ radical with further molecular O_2, and leads to a second C-H activation step that yields 2-hexene and the peroxy radical ($\cdot OOH$). The other pathway is associated with hydrogen transfer from the $\cdot OOH$ radical to $C_6H_{13}OH$ that is produced earlier, leading to water and the alkyl peroxy radical ($C_6H_{13}OO\cdot$). The $C_6H_{13}OO\cdot$ radical undergoes intramolecular H-abstraction to yield 2-hexene and the $\cdot OOH$ radical, and the latter disproportionate through intermediate $\cdot OH$ radicals to produce O_2 and H_2O in the termination step.

* Corresponding author e-mail address: damoyi@mut.ac.za

1 Introduction

The range of carbon resources used by the chemicals industry is set to diversify to include natural gas, heavy oils and tars, coal and biomass. It is attractive to use these various materials as the input to a single chemical processing infrastructure by first converting carbon source materials into syngas and then using a Fischer Tropsch (FT) approach to build the alkanes required for fuels. To use this approach for chemicals production requires low energy conversion of the hydrocarbon feedstocks into more valuable products, such as alkenes and aromatics, making this a critical area of research [1-3]. Reactions of long chain alkanes are limited mainly to combustion and cracking because the C-H bond is non-polar, and the formation of radicals through cracking facilitates propagation steps such as hydrogen abstraction and substitution reactions [4].

Presently large amounts of ethene and propene are produced by thermal cracking of a variety of hydrocarbon feedstocks in the presence of steam at high temperatures [5-7]. Since thermal cracking is an endothermic and energy-intensive process, the most common alternatives include the less energy-intensive non-catalytic and catalytic oxidative dehydrogenation (ODH) routes. The use of gaseous oxygen as oxidant yields water as a by-product and provides the thermodynamic driving force which permits the reaction to be conducted at a lower temperature than a simple dehydrogenation without oxygen [8]. Non-catalytic ODH of propane and butane has been reported before [9], [10] and there are significant publications on catalytic ODH of propane and butane [11-14]. There are, however, limited publications on non-catalytic and catalytic ODH of long chain alkanes, including *n*-hexane.

Thermal cracking in the absence and presence of molecular oxygen is known to proceed by a radical mechanism [15-17]. The non-catalytic ODH of propane is believed to proceed in the same way as thermal cracking [18]. Choudhary *et al.* [9] suggested that, in the absence of oxygen, the initiation step in the thermal cracking of propane occurs through the homolysis of a C-C bond at temperatures above 700°C,

$$C_3H_8 = \cdot CH_3 + \cdot C_2H_5 \qquad (1)$$

Formation of the propyl radical ($\cdot C_3H_7$) through C-H bond scission is less likely because the C-H bond energy (+23.8 kcal/mol) is higher than the C-C bond energy (+21.1 kcal/mol). The mechanism of the formation of propyl radicals may involve the attack of other propane molecules by the methyl and ethyl radicals formed in reaction (1). The authors supported Dente and Ranzi [19], that after the initiation step, the majority of the alkane molecules are activated by such radical species and the reactions proceed through complex free-radical chain propagation and termination reactions, leading to the formation of different products, namely, hydrogen, methane, higher alkanes, alkenes, and coke.

Burch and Crabb [20] observed that the same reaction in the presence of oxygen began at a temperature about 75°C lower than in the absence of oxygen. They further suggested that the presence of oxygen in the gas phase allows additional reaction pathways involving oxygen centred radicals, for example,

$$\cdot C_3H_7 + O_2 = C_3H_6 + HO_2 \cdot \qquad (2)$$

$$\cdot C_2H_5 + O_2 = C_2H_4 + HO_2 \cdot \qquad (3)$$

$$HO_2 \cdot + C_3H_8 = \cdot C_3H_7 + H_2O_2 \qquad (4)$$

$$H_2O_2 = 2HO \cdot \qquad (5)$$

$$C_3H_8 + HO\cdot = \cdot C_3H_7 + H_2O \quad (6)$$

The contribution of molecular oxygen was also discussed in the study of the non-catalytic ODH of butane by Toledo el al [16]. They proposed that one possible initiation step, besides cracking, is the abstraction of a hydrogen atom from a butane molecule by molecular oxygen to form the butyl ($\cdot C_4H_9$) and hydroperoxy ($HO_2\cdot$) radicals. The biradical character of the triplet molecular oxygen facilitates the initiation of a free-radical chain mechanism as follows,

$$C_4H_{10} + O_2 = \cdot C_4H_9 + HO_2\cdot \quad (7)$$

$$C_4H_{10} + HO_2\cdot = \cdot C_4H_9 + H_2O_2 \quad (8)$$

$$C_4H_{10} = \cdot C_2H_5 + \cdot C_2H_5 \quad (9)$$

$$C_4H_{10} = \cdot C_3H_7 + \cdot CH_3 \quad (10)$$

The participation of molecular oxygen was further reported by Pitz and Westbrook [21]. Their kinetic data showed that the activation energy of reaction (7) (+49 kcal/mol) is lower than that of reactions (9) (+85 kcal/mol) and (10) (+81 kcal/mol). Other authors, Liu et al. [22], Lemonidou et al. [10] and Vislovskiy et al. [23], have also reported the homogeneous activation of n-hexane via hydrogen abstraction by gas phase diatomic oxygen.

Hunter et al. [24] proposed that the initiation step for thermal cracking of n-hexane in the absence of oxygen was the C-C bond fission to form two radicals, with C-C rupturing occurring between the most highly substituted carbons atoms. We believe that the presence of oxygen in the same reaction would provide for the possibility of the initiation step being the hydrogen abstraction by molecular oxygen as observed with shorter chain alkanes [21].

The work presented in this publication seeks to establish the overall likely mechanistic pathways in the reaction of *n*-hexane and related intermediates with O_2, $\cdot OH$ and $HO_2\cdot$ radicals to form 1- and 2-hexene under experimental conditions. Note that 3-hexene is not observed in our laboratory experiments nor reported in literature. Most similar reported work in modelling involves catalytic systems and shorter chain hydrocarbons [25-27]. As a result there are limited publications on DFT modelling of gas-phase hydrogen abstraction reactions of long chain alkanes. We, however, focussed on the DFT gas-phase non-catalytic radical mechanisms in order to gain insight and acquire a theoretical baseline for modelling the heterogeneous catalytic (VMgO) ODH reaction of *n*-hexane to benzene at a later stage. This is necessary because in certain catalytic experimental conditions, gas-phase ODH mechanisms may compete with the catalytic ODH mechanisms. We believe that the DFT calculations and comparisons of some kinetic and thermodynamic properties for this reaction will be insightful for better understanding of the reaction mechanisms of the indicated radicals with *n*-hexane and related intermediates.

2 Theoretical Methodology

2.1 Reaction Scheme for *n*-Hexane to 2-Hexene

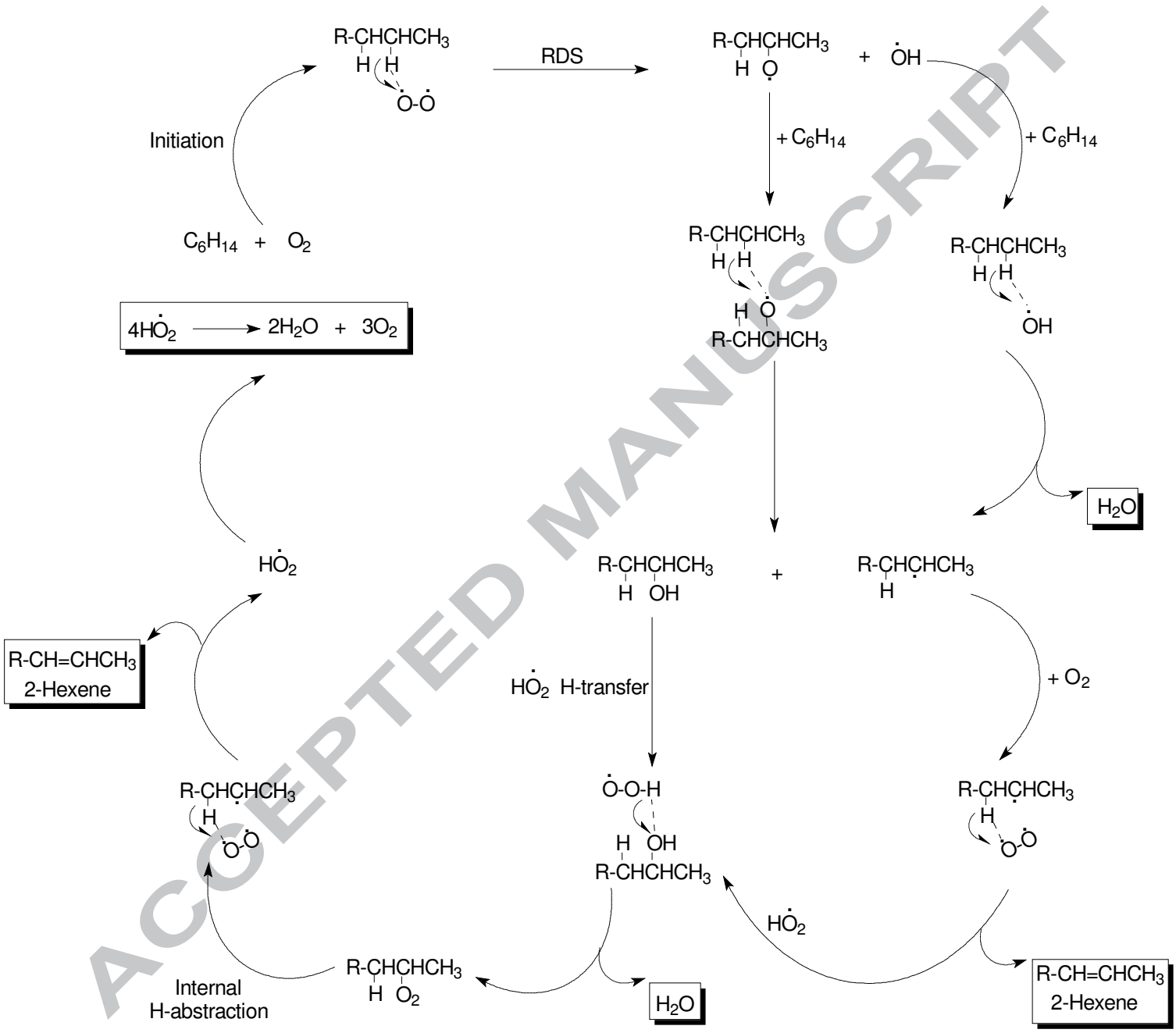

Figure 1 Proposed reaction scheme, with R=$CH_2CH_2CH_3$.

The proposed reaction scheme shown in Figure 1 indicates the formation of 2-hexene from gas-phase ODH of *n*-hexane. Hoog *et al.* [28] investigated this reaction and concluded that an equilibrium exists between 1- and 2-hexene in the reactor. Nevertheless, for clarity purposes we only show the formation of 2-hexene.

Initiation of the reaction involves H-abstraction from the central carbons of the *n*-hexane chain by molecular oxygen which then undergoes O-O scission in the RDS. This follows the formation of a new C-O bond at the activated carbon to give an alkoxy radical species and a hydroxyl radical. The hydroxyl radical may then activate further *n*-hexane molecules to give carbon centred radicals following the formation of water. The alkoxy radical can also activate *n*-hexane to give a secondary alcohol and a carbon centred radical. Interaction of the carbon centred radicals with molecular oxygen can then lead directly to 2-hexene via a second C-H activation event with the production of a hydroperoxyl radical species. The hydroperoxyl radical itself is also capable of additional reaction steps, most notably combining with the alcohol produced earlier in the mechanism to give water and an alkyl peroxy radical which can internally decompose to 2-hexene, reforming the peroxy radical for further reaction. Eventually termination of the radical processes may occur through disproportionation of the hydroperoxyl radicals into water and oxygen.

The overall reaction is,

$$3C_6H_{14} + 3O_2 = 3C_6H_{12} + 2HO_2\cdot + 2H_2O \qquad (11)$$

The intermediate $HO_2\cdot$ radicals produced in reaction (11) may combine as presented in reaction (12),

$$4HO_2\cdot = 2H_2O + 3O_2 \qquad (12)$$

The relative hydrogen abstraction abilities of molecular O_2, the ·OH and $HO_2\cdot$ radicals were examined for activation of *n*-hexane through likely intermediates to 1- and 2-hexene. The activation energies (*E*a), total energy changes (ΔE) and Gibbs free energy changes (ΔG) at different temperatures were calculated and compared.

2.2 Computational Details

The geometries of all stationery points were optimized using the restricted and unrestricted B3LYP/6-311+G(d,p) level of theory. The B3LYP is a hybrid functional that is made up of Becke's three-parameter nonlocal hybrid exchange potential [29] and the nonlocal correlation functional of Lee, Yang and Parr [30]. All the calculations were performed using the Gaussian09 code [31] incorporating the Gausview5.0 graphics interface. The conditions chosen were those used by our group in laboratory experiments, namely 573, 673 and 773 K. Geometry optimizations were carried out without symmetry constraints. The harmonic vibrational frequencies of all the stationary points in potential energy surfaces were calculated at the same level of theory used for their geometry optimizations in order to confirm local minima and transition states, and also determine the corresponding zero-point vibrational energy (ZPVE). The intrinsic reaction coordinate (IRC) [32], [33] calculations were conducted in order to confirm that all transition states connect the relative minima. Stability calculations were performed for all reactants and products so as to determine whether the lowest energy is a restricted or unrestricted wavefunction and natural bond orbital (NBO) [34], [35] analyses were conducted in order to gain insight into the bonding properties of all the stationary points.

3 Results

3.1 Activation of *n*-hexane

The activation of *n*-hexane by O_2 and the two radicals, ·OH and HO_2· was investigated over the three temperatures 573, 673 and 773K in order to contrast the relative energetics involved. All the Gaussian optimised structures of reactants, intermediates, transition states and products/intermediates are included as supplementary material.

Figure 2A displays the relative energy-reaction coordinate pathways for the reaction involving molecular O_2 on a triplet potential energy surface (PES). All the values of the calculated energetics, *E*a, ΔE and ΔG are recorded in Table 1.

The initiation step for the reaction is the interaction of the only two precursors, *n*-hexane and triplet O_2. The highest calculated barrier (the rate-determining step) corresponds to a β-hydrogen abstraction by O_2 with a barrier height of +42.4 kcal/mol (TS_1), relative to separate reactants, utilizing the B3LYP functional. We compared this activation energy with the one calculated using the M06-2X functional [36] in order to investigate the degree of underestimation due to self-interaction errors when utilizing the B3LYP functional [37]. We calculated a barrier of +44.3 kcal/mol for the rate-determining step using the M06-2X functional, indicating an underestimation of 1.9 kcal/mol. Nevertheless, we decided to continue with utilizing the B3LYP functional for this non-catalytic reaction in order to compare the same reaction under catalytic conditions with this recommended functional. These results are in agreement with our expectations from the discussion of the mechanism in Figure 1. The calculated C-H activation by O_2 is accompanied by a decrease in the O--H interaction distance from 3.40Å in the pre-reaction complex to 1.06Å in the TS. The calculated activation energy is comparable to a barrier of +49 kcal/mol that was reported by Pitz and Westbrook [21] for the reaction of O_2 and *n*-butane. Three possible intermediates resulting from this C-H activation process were considered: Int_1 corresponds to the formation of an alkoxy hydroxyl radical pair, Int_2 an alcohol and free oxygen atom and Int_3 a carbon centred radical species with a peroxy radical. The relative thermodynamic energies of these triplet intermediates were calculated (Figure 2A). Although none of the intermediates are thermodynamically stable, relative to reactants, Int_1 is the most stable of the three, with ΔE = +20.5 kcal/mol followed by Int_2 with ΔE = +28.9 kcal/mol, relative to separate reactants. As expected on a triplet PES, the O--O bond distance in Int_1 is 2.23Å, reflecting a weak interaction between the two oxygen-containing radicals, $C_6H_{13}O$· and ·OH. Therefore, the ·OH radicals that may be produced in the pathway through Int_1 are expected to dominate in reactions involving the propagation steps.

The highly energetic Int_3 with ΔE = +44.8 kcal/mol is the most thermodynamically unstable indicating that the reverse reaction for the formation of reactants O_2 and *n*-hexane is kinetically and thermodynamically more favourable (Figure 2A). This is expected because the O-H bond dissociation energy in the HO_2· radical is +47 kcal/mol, which is lower than that in the ·OH radical, namely +103 kcal/mol, and typical C-H bond energies that are *ca.* +100 kcal/mol, [38],[39]. This observation indicates that H-transfer reactions may occur from the HO_2· radical to other electron-deficient species, as also suggested by Anglada *et al.* [40] and Clifford *et al.* [41]. However, the direct formation of a carbon centred radical based solely on the reaction with dioxygen is unlikely to be important in the pathway to alkene formation.

From Figure 2A we conclude that the propagation pathways to the formation of 1- and 2-hexene are likely to proceed through the lowest energy intermediate Int_1, comprising $C_6H_{13}O$· + ·OH radicals. The two radicals may participate in β-hydrogen abstraction reactions from further *n*-hexane molecules through the following steps,

$$C_6H_{14} + C_6H_{13}O\cdot = C_6H_{13}OH + \cdot C_6H_{13} \quad (13)$$

$$C_6H_{14} + HO\cdot = H_2O + \cdot C_6H_{13} \quad (14)$$

Reaction (13) involves the formation of a stable alcohol and hexyl radical. It is necessary to mention that no alcoholic products are observed in our laboratory experiments for this reaction. This means that the alcohol that may form is likely to be the intermediate for the production of olefins. As illustrated in the energy diagram in Figure 2B, the calculated barrier for this step is +8.7 kcal/mol (TS_2), and the indicated intermediate (Int_4) stabilizes to ΔE = -1.8 kcal/mol, relative to reactants. The O--H interaction distance in the TS is 1.29Å and this decreases in the intermediate to 0.97Å, indicating the formation of an alcohol. In the case of reaction (14) we calculated a barrier of +14.6 kcal/mol (TS_5) and the energy difference, ΔE = -18.0 kcal/mol, relative to reactants, as illustrated in Figure 2C. The thermodynamic stability of the reaction is as a result of water being produced as a product.

The formation of 1- and 2-hexene by the reaction of the radical intermediate produced in reactions (13) and (14), with molecular O_2 may proceed either through consecutive reaction steps (15) and (16), or step (17), namely,

$$\cdot C_6H_{13} + O_2 = C_6H_{13}OO\cdot \quad (15)$$

$$C_6H_{13}OO\cdot = C_6H_{12} + HO_2\cdot \quad (16)$$

$$\cdot C_6H_{13} + O_2 = C_6H_{12} + HO_2\cdot \quad (17)$$

In studies involving ethylene and oxygen, Gutman *et al.* [42], [43] found that reacting oxygen with ethyl radicals leads predominantly to the alkene at higher temperatures, and the mechanism involves intramolecular H-abstraction followed by elimination of the hydroperoxyl radical. Similarly, reaction (15) and (16) are, consecutively, chemisorption of O_2 on to the $\cdot C_6H_{13}$ radical to produce the alkyl peroxy radical, $C_6H_{13}OO\cdot$, which undergoes 1,4 intramolecular H-abstraction on α- (1-hexene) and γ- (2-hexene) carbon atoms followed by elimination of the hydroperoxyl radical to produce 1- and 2-hexene. For the two reactions we calculated barriers of +2.6 kcal/mol and +24.4 kcal/mol and energy differences of ΔE = -30.2 kcal/mol and -10.5 kcal/mol for the formation of 2-hexene, respectively (Table 1 – TS_9 and TS_{10}). However, our calculations show a barrierless pathway that is similar to TS_3 (-4.5 kcal/mol) for reaction (17), which is a direct H-abstraction in C3 to produce 2-hexene and the hydroperoxyl radical, as indicated in both Figures 2B and 2C. This pathway produces the required 2-hexene (P_1 and P_3) with ΔE = -11.5 kcal/mol. This is accompanied by a decrease in C-C bond length from 1.39Å in the TSs to 1.34Å in the products, which is comparable to experimental C-C bond lengths of alkenes, namely 1.33 +/- 0.01Å. Therefore the formation of alkenes is likely to proceed by the elementary propagation step (17) rather than the two consecutive propagation steps (15) and (16). Thus, this barrier-less, kinetically and thermodynamically favourable mechanistic pathway is one of the key propagation steps that is likely to dominate in the production of the alkenes and also simultaneously increase the concentration of the $HO_2\cdot$ radicals.

Since no alcoholic products are obtained in our experiments, we then investigated the likely conversion of $C_6H_{13}OH$ obtained in reaction (13) to C_6H_{12}. The pathway investigated is H-transfer from $HO_2\cdot$ obtained in reaction (17) to produce the hexyl radical, water and oxygen,

$$C_6H_{13}OH + HO_2\cdot = \cdot C_6H_{13} + H_2O + O_2 \quad (18)$$

As illustrated in Figure 2D, we calculated an energy barrier of +29.4 kcal/mol (TS_8) for this step, however, the intermediate obtained was $C_6H_{13}OO\cdot$ rather than $\cdot C_6H_{13}$, with ΔE = -8.6 kcal/mol (Int_6). Other studies [44], [45] also confirm the higher thermodynamic stability of $C_6H_{13}OO\cdot$ compared to that of $\cdot C_6H_{13}$. The formation of the stable H_2O is facilitated by advanced scission of the CO (2.17Å) and OH (1.53Å) bonds in the TS for $C_6H_{13}OH$ and $HO_2\cdot$, respectively. As discussed above in reaction (16), the alkyl peroxy radical, $C_6H_{13}OO\cdot$ may undergo intramolecular H-abstraction, and we calculated a barrier (TS_9) of +24.4 kcal/mol for this step. This is followed by a 1,5 elimination to produce 2-hexene and the hydroperoxyl radical, with ΔE = -10.5 kcal/mol (P_5).

The prominent feature of the $\cdot C_6H_{13}$ radical in our calculations obligated the examination of the intramolecular H-elimination pathway to produce 2-hexene, namely,

$$\cdot C_6H_{13} = C_6H_{12} + H\cdot \qquad (19)$$

Table 2 shows the calculated $\Delta E^{\#}$ value of +36.3 kcal/mol (TS_{11}) and the corresponding ΔE value of +36.5 kcal/mol (Int_7) for the 2-hexene pathway, suggesting that such a reaction is unlikely to occur under the specified conditions.

Finally, the remaining hydroperoxyl radicals may combine to produce the intermediate hydroxyl radicals,

$$2HO_2\cdot = 2HO\cdot + O_2 \qquad (20)$$

The activation barrier for reaction (20) has $\Delta E^{\#}$ = -2.3 kcal/mol (TS_{12}) and the products, $2\cdot OH + O_2$ stabilize to ΔE = -18.8 kcal/mol (Int_8 in Table 1), relative to TS. This suggests that this reaction pathway may be one of those that generate the more reactive ·OH radicals, with the reformation of O_2 also contributing to the stabilization of the products. Moreover, the ·OH and $HO_2\cdot$ radicals that are likely to be produced may also participate in the activation of more *n*-hexane molecules and also the produced 1- and 2-hexenes.

The termination step involves the hydroxyl radicals that combine kinetically and thermodynamically favourably to produce water and oxygen,

$$4HO\cdot = 2H_2O + O_2 \qquad (21)$$

The first step is H-transfer between the two ·OH radicals to produce H_2O and O diradical with $\Delta E^{\#}$ = -4.7 kcal/mol (TS_{13}) and ΔE = -8.3 kcal/mol (Int_9), relative to TS. The second step is the combination of two O diradicals with $\Delta E^{\#}$ = -2.1 kcal/mol (TS_{14}) and ΔE = -115.7 kcal/mol (P_7) relative to TS, for the formation of O_2 (Table 1).

3.2 Temperature Effects

Trends are observed with respect to the Gibbs free energies of activation ($\Delta G^{\#}$) and the Gibbs free energies (ΔG) for all the steps at the indicated temperatures of 573K, 673K and 773K (Table 1).

As expected, the activation of *n*-hexane by O_2 (TS_1) and the H-transfer from $HO_2\cdot$ radical to $C_6H_{13}OH$ (TS_8) pathways have the largest $\Delta G^{\#}$ values as a result of the low reactivity of the triplet O_2 molecule in the first case and the breaking and creation of many bonds in the H-transfer case. The lowest $\Delta G^{\#}$ values are generally observed in reaction pathways that include propagation by O_2 (TS_3, TS_4, TS_6 and TS_7). Similarly the ΔG values, relative to separate reactants in each case, become less negative (more positive)

as the temperature increases from 573 to 773K, suggesting that the reaction steps become less thermodynamically favourable with increase in temperature. Again, as predictable, our calculations reflect small changes in entropy factors, $\Delta S^{\#}$ and ΔS, as the temperature changes for all the steps, suggesting that all the thermodynamically favourable reactions are driven by negative enthalpy changes, ΔH. Of note is the conversion of $2HO_2\cdot$ radicals to $2\cdot OH$ radicals and O_2 (TS_{11}), where the reaction becomes slightly more thermodynamically favourable from 573 to 773K. Clearly, for this reaction pathway ΔS is positive at any temperature and our calculations show that the former remains constant with increase in temperature. Therefore, ΔG becomes slightly more negative with increase in temperature because ΔH follows the same trend.

Clearly, the most kinetically and thermodynamically favourable pathways are for the propagation steps associated with the O_2 molecule.

3.3 Natural Bond Orbital Analyses

Natural bond orbital (NBO) analysis provides an efficient method for studying intra- and intermolecular bonding, interaction among bonds and also provides a convenient basis for investigating charge transfer or conjugative interaction in molecular systems [46]. NBO analyses were performed on the stationary points (TS) of the most likely mechanistic pathways at the B3LYP/6-311+G(d,p) level. The TSs and the corresponding highest occupied NBOs (HONBOs), representing donor orbitals, and lowest unoccupied NBOs (LUNBOs), representing acceptor orbitals, are displayed in Figure 3. Only the TSs and NBOs associated with 2-hexene (TS_3) and 1-hexene (TS_4) in the earlier pathways are illustrated and those in later pathways (TS_6 for 2-hexene) and (TS_7 and 1-hexene) are omitted because of similarities. However, Table 2 lists all the TSs, NBOs, atomic charges and largest orbital energies for each TS.

For the initiation step (TS_1), the abstraction of H by O_2 corresponds to the largest interaction that comprises the Lewis-type highest occupied NBO (HONBO) that comprises a C *s*(7.1%) *p*(92.9%) nonbonding-type hybrid as the donor orbital. The numbers in % indicate the contribution of each orbital to the NBO hybrid. The acceptor orbital is the non-Lewis-type lowest unoccupied NBO (LUNBO) that is the H *s*(76.3%) and O *s*(6.9%) *p* (16.8%) antibonding hybrid. The HONBO donates electron density to the LUNBO with orbital stabilization energy of +38.2 kcal/mol, thereby facilitating the formation of a new HO bond. The largest negative charge among the three interacting atoms is on the O atom (-0.277) and the positive charge on the H atom (+0.423), indicating qualitatively, a relatively stronger interaction between the two atoms. The interaction is between the O *s*(28.0%) *p*(72.0%) nonbonding hybrid orbital (HONBO) that donates electron density to the H *s* (71.9%) and C *s*(5.5%) *p*(22.6%) antibonding hybrid (LUNBO). phases of the lobes. For TS_2, the largest orbital energy is +45.6 kcal/mol. The corresponding atomic charges on the three interacting atoms are C = -0.275, H = +0.312 and O = -0.567. We calculated the orbital energy of +42.1 kcal/mol for the formation of 2-hexene (TS_3 and TS_6) through the O_2 propagation pathways. The flow of electron density is from the O *s*(13.1%) *p*(86.9%) nonbonding hybrid to the H *s* (71.1%) and C *s*(3.4%) *p*(25.5%) antibonding hybrid. Similarly, for 1-hexene (TS_4 and TS_7) electron density flows from the O *s*(13.3%) *p*(86.7%) nonbonding hybrid to the H *s* (71.4%) and C *s*(3.7%) *p* (24.9%) antibonding hybrid. The distribution of atomic charges in interacting atoms follows the same trend with negative charges on C and O atoms and positive charges on the H atoms. In all these cases, further electron density directional flow is a result of the LUNBOs delocalizing principally to vicinal CC antibonding orbitals to facilitate π-bond formation. The donor-acceptor orbitals for TS_5 are the O *s*(27.3%) *p*(72.7%) nonbonding hybrid and the H *s* (66.6%) and C *s*(7.7%) *p* (25.7%) antibonding hybrid with atomic charges on involved atoms being C = -0.478, H = +0.0257 and O = -0.613. For TS_8 two HONBOs and LUNBOs were identified corresponding to H-transfer from (HO_2) the O *s*(15.1%) *p* (84.9%) nonbonding hybrid to ($C_6H_{13}OH$) H *s*(78.9%) and O *s*(4.9%) *p* (16.2%) antibonding hybrid, and the OH scission from $C_6H_{13}OH$ with the O *s*(35.6%) *p*(64.4%) nonbonding hybrid transferring electron

density to (C_6H_{13}) the C *s*(1.0%) *p* (99.0%) antibonding hybrid. The associated orbital energies are +21.3 and +22.0 kcal/mol, respectively. Examination of the TS reveals that this step follows a concerted mechanistic pathway that involves OH scission from $C_6H_{13}OH$ accompanied by H_2O formation. Lastly, TS_9 and TS_{10} represent the formation of 2- and 1-hexene from intramolecular H-abstraction in $C_6H_{13}OO\cdot$, respectively, and in both cases the donor orbitals are the O *s*(13.1%) *p*(86.9%) and the O *s*(13.4%) *p*(86.6%) nonbonding hybrids and the acceptor orbitals are the H *s*(70.8%) and C *s*(3.5%) *p*(25.7%), and the H *s*(70.2%) and C *s*(4.0%) *p*(25.8%) with orbital interaction energies of +39.3 and +43.5 kcal/mol.

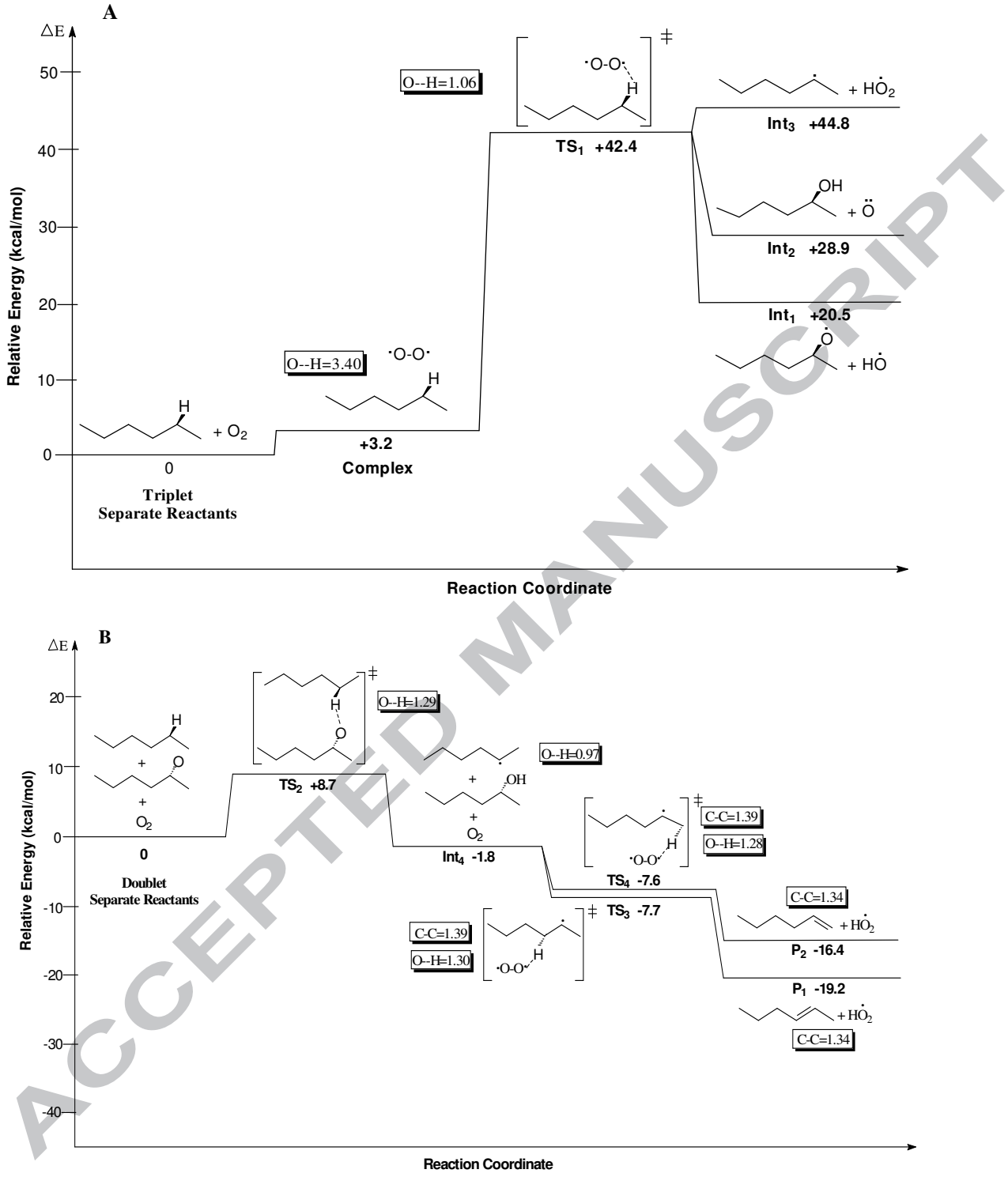

Figure 2 Zero-point corrected relative electronic energy (Δ*E*) diagrams for the reaction of *n*-hexane to 1- and 2-hexene. Scheme A is the activation of *n*-hexane to intermediates. Scheme B is the propagation pathway involving the $C_6H_{13}O^{\cdot}$ radical from Int_1, viz. Reaction (13) and (17). The indicated bond distances are in Å. B3LYP/6-311+g(d,p) for the C, O and H atoms. Cartesian coordinates of all TSs are provided as supplementary material.

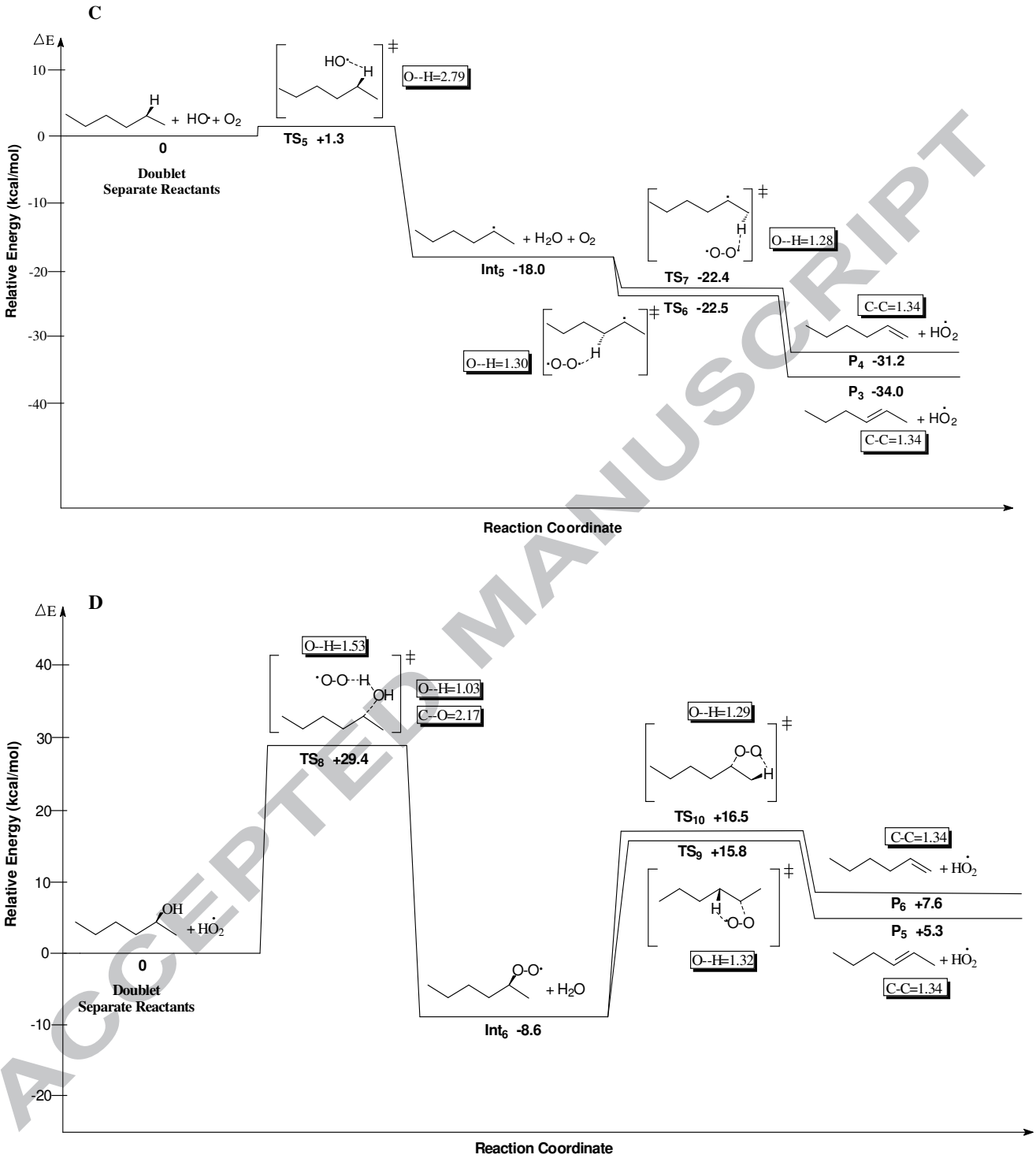

Figure 2 Continuing Scheme C is the propagation pathway involving the OH radical from Int_1, viz. reaction (14) and (17). Scheme D is the propagation pathway involving the alcohol obtained from reaction (13) and HO_2 radical, viz. reaction (18). B3LYP/6-311+g(d,p) for the C, O and H atoms. Cartesian coordinates of all TSs are provided as supplementary material.

Table 1: Relative Energies (Δ*E*) and Gibbs Free Energies (Δ*G*) for the reaction of *n*-hexane with molecular O_2[a]. B3LYP/6-311+g(d,p) for the C, O and H atoms. Cartesian coordinates of all TSs are provided as supplementary material.

Reaction Pathway	Δ*E*	Δ*G*		
		573	673	773
Initiation				
***t*-O_2+*n*-C_6H_{14}**	0	0	0	0
***t*-O_2--*n*-C_6H_{14} (TS_1)**	+42.4	+53.6	+55.8	+57.9
***t*-TS_1→HO+$C_6H_{13}O$ (Int_1)**	+20.5 (-21.9)	+31.8 (-21.8)	+34.0 (-21.8)	+36.2 (-21.7)
***t*- TS_1→O+$C_6H_{13}OH$ (Int_2)**	+28.9 (-13.5)	+35.7 (-17.9)	+38.0 (-17.8)	+40.3 (-17.6)
***t*- TS_1→HO_2+C_6H_{13} (Int_3)**	+44.8 (+2.4)	+51.9 (-1.7)	+53.4 (-2.4)	+54.8 (-3.1)
Propagation from Int_1 ($C_6H_{13}O$)				
***d*-$C_6H_{13}O$+*n*-C_6H_{14}**	0	0	0	0
***d*-$C_6H_{13}O$--*n*-C_6H_{14} (TS_2)**	+8.7	+25.6	+28.3	+31.9
***d*-TS_2→$C_6H_{13}OH$+C_6H_{13} (Int_4)**	-1.8 (-10.5)	+6.7 (-18.9)	+8.5 (-19.8)	+10.2 (-21.7)
***d*-Int_4→O_2--C_6H_{13} (TS_3)**	-7.7 (-5.9)	+10.5 (+3.8)	+13.9 (+5.4)	+17.3 (+7.1)
***d*-TS_3→HO_2+C_6H_{12} (P_1): 2-hexene**	-19.2 (-11.5)	-9.8 (-20.3)	-7.9 (-21.8)	-6.1 (-23.4)
***d*-Int_4→O_2--C_6H_{13} (TS_4)**	-7.6 (-5.8)	+10.7 (+4.0)	+14.2 (+5.7)	+17.6 (+7.4)
***d*-TS_4→ HO_2+C_6H_{12} (P_2): 1-hexene**	-16.4 (-8.8)	-6.9 (-17.6)	-5.0 (-19.2)	-3.1 (-20.7)
Propagation from Int_1 (HO)				
***d*-HO+*n*-C_6H_{14}**	0	0	0	0
***d*-HO--*n*-C_6H_{14} (TS_5)**	+14.6	+28.1	+30.5	+32.7
***d*-TS_5→ H_2O+C_6H_{13} (Int_5)**	-18.0 (-32.6)	-13.1 (-41.3)	-12.0 (-42.5)	-10.9 (-43.6)
***d*-Int_5→O_2--C_6H_{13} (TS_6)**	-22.5 (-4.5)	-5.7 (+7.4)	-2.6 (+9.4)	+0.6 (+11.5)
***d*-TS_6→HO_2+C_6H_{12} (P_3): 2-hexene**	-34.0 (-11.5)	-26.0 (-20.3)	-24.3 (-21.7)	-22.7 (-23.3)
***d*-Int_5→O_2--C_6H_{13} (TS_7)**	-22.4 (-4.4)	-5.4 (+7.7)	-2.2 (+9.8)	+1.0 (+11.9)
***d*-TS_7→HO_2+C_6H_{12} (P_4): 1-hexene**	-31.2 (-8.8)	-23.1 (-17.7)	-21.4 (-19.2)	-19.8 (-20.8)
Propagation – H-transfer				
***d*-HO_2+$C_6H_{13}OH$**	0	0	0	0
***d*-HO_2--$C_6H_{13}OH$ (TS_8)**	+29.4	+44.9	+47.9	+50.8
***d*-TS_8→H_2O+$C_6H_{13}OO$ (Int_6)**	-8.6 (-38.0)	+1.7 (-43.2)	+3.8 (-44.1)	+5.8 (-45.0)
***d*-$C_6H_{13}OO$ (TS_9) Intra H-abstraction**	+15.8 (+24.4)	+26.7 (+25.0)	+28.8 (+25.0)	+30.8 (+25.0)
***d*-TS_9→HO_2+C_6H_{12} (P_5): 2-hexene**	+5.3 (-10.5)	+7.8 (-18.9)	+8.5 (-20.3)	+9.2 (-21.6)
***d*-$C_6H_{13}OO$ (TS_{10}) Intra H-abstraction**	+16.5 (+25.1)	+26.9 (+25.2)	+29.1 (+25.3)	+31.2 (+25.4)
***d*-TS_{10}→HO_2+C_6H_{12} (P_6): 1-hexene**	+7.6 (-8.9)	+12.3 (-14.6)	+9.3 (-19.8)	+15.0 (-16.2)
Intra H-elimination				
***d*-·C_6H_{13}**	0	0	0	0
***d*-·C_6H_{13} (TS_{11})**	+36.3	+37.4	+37.6	+37.8
***d*-TS_{11}→C_6H_{12} + H· (Int_7): 2-hexene**	+36.5 (+0.2)	+30.6 (-6.8)	+29.5 (-8.1)	+28.5 (-9.3)
Termination				
***s*-HO_2+HO_2**	0	0	0	0
***s*-HO_2--HO_2 (TS_{12})**	-2.3	+4.9	+5.8	+6.7
***s*-TS_{12}→2HO+O_2 (Int_8)**	-21.1 (-18.8)	-23.4 (-28.3)	-24.1 (-29.9)	-24.9 (-31.6)
***t*-HO--HO (TS_{12})**	-4.7	+8.5	+11.0	+13.6
***t*-TS_{13}→H_2O+O (Int_9)**	-13.0 (-8.3)	-3.2 (-11.7)	-1.3 (-12.3)	+0.7 (-12.9)
***t*-O--O (TS_{14})**	-2.1	+10.7	+13.1	+15.6
***t*-TS_{14}→O_2 (P_7)**	-117.8 (-115.7)	-104.2 (-114.9)	-101.6 (-114.7)	-99.0 (-114.6)

[a] **Δ*E* and Δ*G* are zero-point corrected electronic energy and Gibbs free energy at standard pressure, relative to separate reactants respectively, in kcal/mol. The energies in parentheses are for the indicated reaction pathways. The temperature is in K and Δ*E* values are at 673K. Prefixes *t*-, *d*- and *s*- indicate triplet, doublet and singlet states, respectively.**

Table 2: NBO atomic charges, HONBO and LUNBO orbital types, and largest orbital energies for the TSs of the *n*-hexane to 1- and 2-hexene pathways. B3LYP/6-311+g(d,p) for all the atoms. Cartesian coordinates of all TSs are provided as supplementary material.

Transition state	Atomic charges on interacting atoms	HONBO type	LUNBO type	Orbital Stabilization Energy (kcal/mol)
1	C = -0.191 H = +0.423 O = -0.277	C *s*(7.1%) *p*(92.9%) nonbonding hybrid	H *s*(76.3%) O *s*(6.9%) *p*(16.8%) antibonding hybrid	+38.2
2	C = -0.275 H = +0.312 O = -0.567	O *s*(28.0%) *p*(72.0%) nonbonding hybrid	H *s*(71.9%) C *s*(5.5%) *p*(22.6%) antibonding hybrid	+45.6
3 and 6	C = -0.478 H = +0.360 O = -0.225	O *s*(13.1%) *p*(86.9%) nonbonding hybrid	H *s*(71.1%) C *s*(3.4%) *p*(25.5%) antibonding hybrid	+42.1
4 and 7	C = -0.387 H = +0.192 O = -0.408	O *s*(13.3%) *p*(86.7%) nonbonding hybrid	H *s*(71.4%) C *s*(3.7%) *p*(24.9%) antibonding hybrid	+45.9
5	C = -0.478 H = +0.257 O = -0.613	O *s*(27.3%) *p*(72.7%) nonbonding hybrid	H *s*(66.6%) C *s*(7.7%) *p*(25.7%) antibonding hybrid	+23.6
8	C = -0.170 O (O_2) = -0.888 H = +0.480 O (OH) = -0.277	O *s*(35.6%) *p*(64.4%) and O *s*(15.1%) *p*(84.9%) nonbonding hybrids	H *s*(78.9%) O *s*(4.9%) *p*(16.2%) and C *s*(1.0%) *p*(99.0%) antibonding hybrid	+21.3 and +22.0
9	C = -0.486 H = +0.363 O = -0.218	O *s*(13.1%) *p*(86.9%) nonbonding hybrid	H *s*(70.8%) C *s*(3.5%) *p*(25.7%) antibonding hybrid	+39.3
10	C = -0.667 H = +0.361 O = -0.215	O *s*(13.4%) *p*(86.6%) nonbonding hybrid	H *s*(70.2%) C *s*(4.0%) *p*(25.8%) antibonding hybrid	+43.5

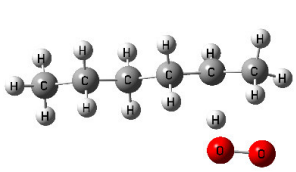

TS1

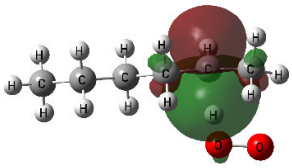

HOMO

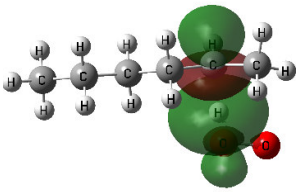

LUMO

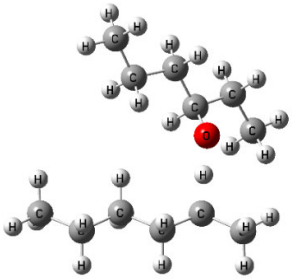

TS2

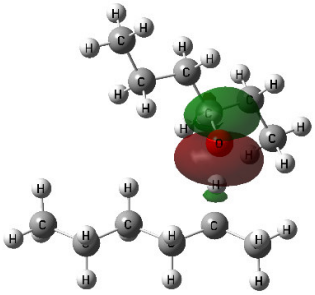

HOMO

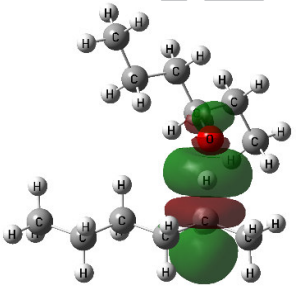

LUMO

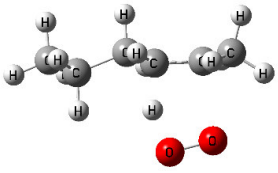

TS3

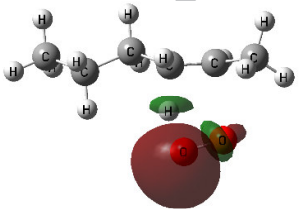

HOMO

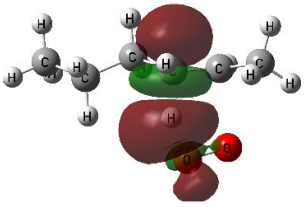

LUMO

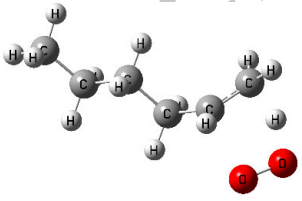

TS4

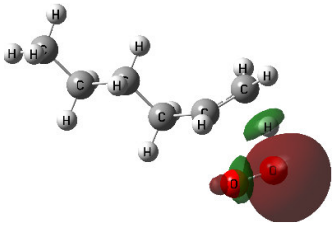

HOMO

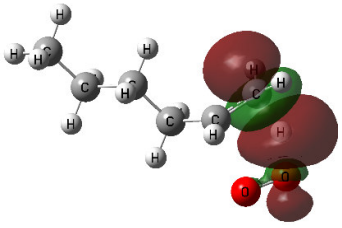

LUMO

Figure 3A Transition state structures and frontier orbitals for the likely mechanistic scheme. The orbital lobes are oriented for better clarity in each case and correspond to the reaction coordinate.

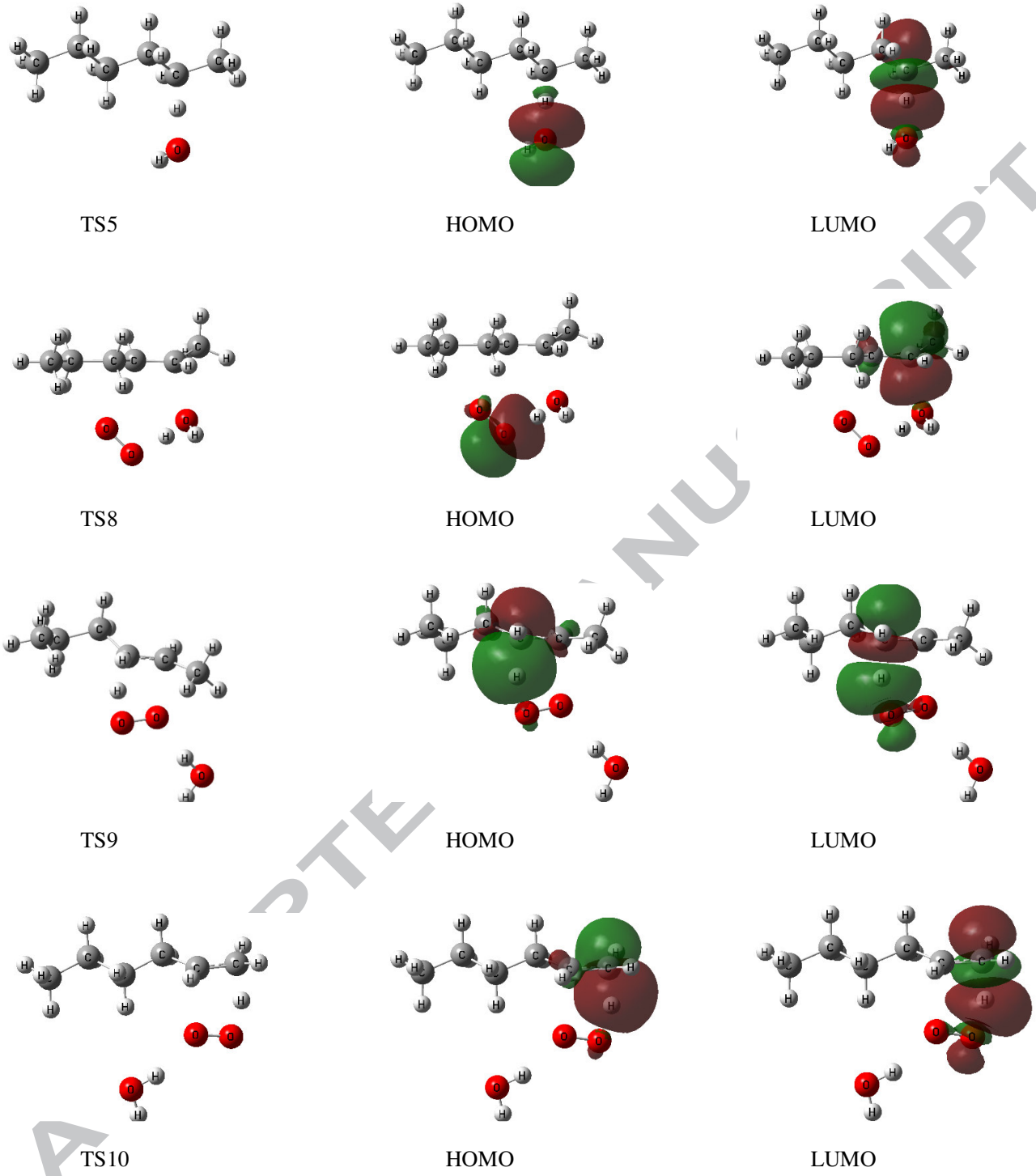

Figure 3B Transition state structures and frontier orbitals for the likely mechanistic scheme. The orbital lobes are oriented for better clarity in each case and correspond to the reaction coordinate.

4 Conclusions

The mechanism for activation of *n*-hexane by molecular oxygen and subsequent propagation pathways is proposed based on DFT modelling using experimental conditions of 573, 673 and 773K. All the pathways are recorded in Table 1.

The formation of CO_x was not considered for this study. The most kinetically and thermodynamically favourable mechanistic pathways that are likely to drive the reaction are the following,

- Initiation: $C_6H_{14} + O_2 = C_6H_{13}O\cdot + HO\cdot$

Since O_2 and *n*-hexane are the only species present at the initial stages of the reaction, the rate-determining step is the abstraction of H from *n*-hexane by triplet O_2 with a barrier height of +42.4 kcal/mol. The pathway stabilizes to produce the intermediate (Int_1) that comprises the alkoxy ($C_6H_{13}O\cdot$) and hydroxyl ($HO\cdot$) radicals. This intermediate is thermodynamically more stable (ΔE = +20.5 kcal/mol) than that composed of the alkyl ($C_6H_{13}\cdot$) and hydroperoxy radicals ($HO_2\cdot$), with ΔE = +44.8 kcal/mol, relative to separate reactants. (Figure 2A).

- Propagation by $HO\cdot$ and $C_6H_{13}O\cdot$: $C_6H_{14} + HO\cdot = H_2O + \cdot C_6H_{13}$

  $C_6H_{14} + C_6H_{13}O\cdot = C_6H_{13}OH + \cdot C_6H_{13}$

H-abstraction from further *n*-hexane molecules by $\cdot OH$ and $C_6H_{13}O\cdot$ radicals. The indicated first step has a barrier of +14.6 kcal/mol and the second step +8.7 kcal/mol. The intermediates stabilize with associated ΔE values of -18.0 and -1.8 kcal/mol, respectively (Figures 2B and 2C).

- Propagation by O_2: $\cdot C_6H_{13} + O_2 = C_6H_{12} + HO_2\cdot$

H-abstraction from the generated $\cdot C_6H_{13}$ radicals by molecular O_2. This step is barrierless (-5.9 kcal/mol) and also thermodynamically favourable by -17.4 kcal/mol for the formation of 2-hexene (Figure 2B).

- Propagation by $HO_2\cdot$: $C_6H_{13}OH + HO_2\cdot = C_6H_{13}OO\cdot + H_2O$

A concerted mechanistic pathway that involves H-transfer from $HO_2\cdot$ radical to $C_6H_{13}OH$ that is accompanied by H_2O formation has a barrier height of +29.4 kcal/mol and the reaction step is thermodynamically favourable and produces $C_6H_{13}OO\cdot$ and H_2O with ΔE = -8.6 kcal/mol (Figure 2D).

- Propagation by $C_6H_{13}OO\cdot$: $C_6H_{13}OO\cdot = C_6H_{12} + HO_2\cdot$

Intramolecular H-abstraction and $HO_2\cdot$ elimination to produce 2-hexene with a barrier height of +24.4 kcal/mol and ΔE value of +5.3 kcal/mol from the initial reactants of $HO_2\cdot$ and $C_6H_{13}OH$ (Figure 2D).

Termination:

$$2HO_2\cdot = 2HO\cdot + O_2$$
$$2HO\cdot = H_2O + O$$
$$2O = O_2$$

The remaining $HO_2\cdot$ radicals combine to produce H_2O and O_2 through a series of three steps. For the three steps we calculated barrier-less energies of -2.3, -4.7 and -2.1 kcal/mol, and the corresponding ΔE values of -21.1, -13.0 and -117.8 kcal/mol, relative to separate reactants, respectively (Table 1).

Acknowledgments

This work was supported by the NRF, SASOL and Johnsson Matthey. We would like to thank the Centre for High Performance Computing (CHPC) in Cape Town, South Africa, for providing the computational resources necessary to conduct this work.

References

[1] P. Viparellia, P. Ciambellib, L. Lisic, G. Ruoppoloa, G. Russoa, J. C. Volta, **Oxidative dehydrogenation of propane over vanadium and niobium oxides supported catalysts,** Appl. Catal., A 184 (1999) 291-301.

[2] A.T. Bell, S. Chempath, **A DFT study of the mechanism and kinetics of methane oxidation to formaldehyde occurring on silica-supported molybdena,** J. Catal. 247 (2007) 119-126.

[3] E.A. Elkhalifa, H.B. Friedrich, **Oxidative dehydrogenation of n-octane using vanadium-magnesium oxide catalysts with different vanadium loadings,** Appl. Catal., A 373 (2010) 122-131.

[4] C. Boyadjian, L. Lefferts, K. Seshan, **Catalytic oxidative cracking of hexane as a route to olefins**, Appl. Catal., A 372 (2010) 167-174.

[5] A. Chauvel. G. Lefebvre, **Petrochemical processes: Technical and economic characteristics**, Editions Technip, Paris, 1989.

[6] J.A. Moulijn, M. Makkee, A. van Diepen, **Chemical process technology**, Wiley, Chichester, 2001.

[7] D. Dharia, W. Letzsch, H. Kim, D. McCue, L. Chapin, **Increase light olefins production**, Hydrocarbon Process., Int. Ed. 83 (2004) 61.

[8] H.H. Kung, **Transition metal oxides: Surface chemistry and catalysis**, Stud. Surf. Sci. Catal. 45, Elsevier, Amsterdam, 1989.

[9] V.R. Choudhary, V.H. Rane, A.M. Rajput, **Simultaneous thermal cracking and oxidation of propane to propylene and ethylene**, AlChE J. 44 (1998) 2293-2301.

[10] A.A. Lemonidou, A.E. Stambouli, **Catalytic and non-catalytic oxidative dehydrogenation of n-butane**, Appl. Catal., A 171 (1998) 325-332.

[11] J. Park, C. Shin, **Influence of the catalyst composition in the oxidative dehydrogenation of 1-butene over BiV_xMo_{1-x} oxide catalysts**, Appl. Catal., A 495 (2015) 1-7.

[12] F. Cavani, N. Ballarini, A. Cericola, **Oxidative dehydrogenation of ethane and propane: How far from commercial implementation,** Catal. Today 127 (2007) 113-131.

[13] R. Grabowski, **Kinetics of the oxidative dehydrogenation of propane on vanadia/titania catalysts, pure and doped with rubidium**, Appl. Catal., A 270 (2004) 37-47.

[14] D. Creaser, B. Andersson, R.R. Hudgins, P.L. Silveston, **Transient study of oxidative dehydrogenation of propane**, Appl. Catal., A 187 (1999) 147-160.

[15] R.R. Baker, R.R. Baldwin, R.W. Walker, **Alkene formation in hydrocarbon oxidation**, Elsevier, Amsterdam, 1977.

[16] J.A. Toledo, H. Armendariz, E. L´opez-Salinas, **Oxidative dehydrogenation of n-butane: a comparative study of thermal and catalytic reaction using Fe–Zn mixed oxides**, Catal. Lett. 66 (2000) 19-24.

[17] V.S. Arutyunov, L.N. Strekova, A.V. Nikitin, **Partial oxidation of light alkanes as a base of new generation of gas chemical processes**, Eurasian Chem. Technol. J. 15 (2013) 265-273.

[18] J.E. Taylor, D.M. Kulich, **Industrial and laboratory pyrolysis**, in: L.F. Albright, B.L. Crynes (Eds.), ACS Symposium Series 32, Washington, 1976, pp. 72-83.

[19] M.E. Dente, E. M. Ranzi, **Mathematical modelling of hydrocarbon pyrolysis reactions,** in: L. F. Albright, B. L. Crynes, W. H. Corcoran (Eds.), **Pyrolysis: Theory and industrial practice,** Academic Press, New York, 1983, pp. 133-175.

[20] R. Burch, E.M. Crabb, **Homogeneous and heterogeneous contributions to the oxidative dehydrogenation of propane on oxide catalysts,** Appl. Catal., A 100 (1993) 111-130.

[21] W.J. Pitz, C.K. Westbrook, **Chemical kinetics of the high pressure oxidation of n-butane and its relation to engine knock**, Combus. Flame 63 (1986) 113-133.

[22] X. Liu, W. Li, H. Xu, Y. Chen, **Production of light alkenes with low CO_2 emission from gas phase oxidative cracking (GOC) of hexane**, React. Kinet. Catal. Lett. 81 (2) (2004) 203-209.

[23] V.P. Vislovskiy, T.E. Suleimanov, M.Yu. Sinev, Yu.P. Tulenin, L.Ya. Margolis, V. Cortés Corberán, **On the role of heterogeneous and homogeneous processes in oxidative dehydrogenation of C_3-C_4 alkanes,** Catal. Today 61 (2000) 287-293.

[24] K.C. Hunter, A.L.L. East, **Properties of C-C bonds in *n*-alkanes: Relevance to cracking mechanisms**, J. Phys. Chem. A 106 (2002) 1346-1356.

[25] Y. Liu, Z. Geng, Y. Wang, J. Liu, X. Hou, **DFT studies for activation of C-H bond in methane by gas-phase Rh_n^+ (n = 1 – 3)**, Comput. Theor. Chem. 1015 (2013) 52-63.

[26] K. Alexopoulos, M. Reyniers, G.B. Marin, **Reaction path analysis of propane selective oxidation over V_2O_5 and V_2O_5/TiO_2**, J. Catal. 289 (2012) 127-139.

[27] E. Kurnaz, M.F. Fellah, I. Onal, **A density functional theory study of C-H bond activation of methane on a bridge site of M-O-M-ZSM-5 cluster (M = Au, Ag, Fe and Cu)**, Microporous Mesoporous Mater. 138 (2011) 68-74.

[28] H. Hoog, J. Herheus, F.J. Zuiderweg, **Investigations into the cyclisation (aromatisation) of aliphatic hydrocarbons**, Trans. Faraday Soc. 35 (1939) 993.

[29] A.D. Becke, **Density functional thermochemistry III. The role of exact exchange**, J. Chem. Phys. 98 (1993) 5648.

[30] C. Lee, W. Yang, R.G. Parr, **Development of the Colle-Salvetti correlation energy formula into a functional of the electron density**, Phys. Rev. B 37 (1988) 785.

[31] M.J. Frisch, G.W. Trucks, H.B. Schlegel, G.E. Scuseria, M.A. Robb, J.R. Cheeseman, G. Scalmani, V. Barone, B. Mennucci, G.A. Petersson, H. Nakatsuji, M. Caricato, X. Li, H.P. Hratchian, A.F. Izmaylov, J. Bloino, G. Zheng, J.L. Sonnenberg, M. Hada, M. Ehara, K.

Toyota, R. Fukuda, J. Hasegawa, M. Ishida, T. Nakajima, Y. Honda, O. Kitao, H. Nakai, T. Vreven, J. Montgomery, J. A., J.E. Peralta, F. Ogliaro, M. Bearpark, J.J. Heyd, E. Brothers, K.N. Kudin, V.N. Staroverov, R. Kobayashi, J. Normand, K. Raghavachari, A. Rendell, J.C. Burant, S.S. Iyengar, J. Tomasi, M. Cossi, N. Rega, N.J. Millam, M. Klene, J.E. Knox, J.B. Cross, V. Bakken, C. Adamo, J. Jaramillo, R. Gomperts, R.E. Stratmann, O. Yazyev, A.J. Austin, R. Cammi, C. Pomelli, J.W. Ochterski, R.L. Martin, K. Morokuma, V.G. Zakrzewski, G.A. Voth, P. Salvador, J.J. Dannenberg, S. Dapprich, A.D. Daniels, Ö. Farkas, J.B. Foresman, J.V. Ortiz, J. Cioslowski, D.J. Fox, **Gaussian 09, Revision B.01, Gaussian, Inc.**, Wallingford, 2010.

[32] C. Gonzales, H.B. Schlegel, **An improved algorithm for reaction path following,** J. Chem. Phys. 90 (1989) 2154.

[33] C. Gonzales, H.B. Schlegel, **Reaction path following in mass-weighted internal coordinates**, J. Phys. Chem. 94 (1990) 5523-5527.

[34] J.E. Carpenter, F. Weinhold, **Analysis of the geometry of the hydroxymethyl radical by the "different hybrids for different spins" natural bond orbital procedure,** J. Mol. Struct. THEOCHEM 169 (1988) 41-62.

[35] F. Weinhold, J. E. Carpenter, **The natural bond orbital Lewis structure concept for molecules, radicals, and radical Ions**, in: R. Naaman, Z. Vager (Eds.), **The structure of small molecules and ions**, Plenum, New York, 1988, pp. 227-236.

[36] Y. Zhao, D.G. Truhlar, **The M06 suite of density functionals for main group thermochemistry, thermochemical kinetics, noncovalent interactions, excited states, and transition elements: Two new functionals and systematic testing of four M06-class functionals and 12 other functionals**, Theor. Chem. Acc. 120 (2006) 215-241.

[37] N. Chéron, D. Jacquemin, P. Fleurat-Lessard, **A qualitative failure of B3LYP for textbook organic reactions**, Phys. Chem. Chem. Phys. 14 (2012) 7170-7175.

[38] K.P. Huber, G. Herzberg, **Molecular spectra and molecular structure. Constants of diatomic molecules**, Van Nostrand, New York, 1979.

[39] D.F. McMillen, D.M. Golden, **Hydrocarbon bond dissociation energies**, Annu. Rev. Phys. Chem. 33 (1982) 493-532.

[40] J.M. Anglada, V.M. Domingo, **Mechanism for the gas-phase reaction between formaldehyde and hydroperoxyl radical. A theoretical study**, J. Phys. Chem. A 109 (2005) 10786-10794.

[41] E.P. Clifford, P.G. Wenthold, R. Gareyev, W.C. Lineberger, C.H. DePuy, V.M. Bierbaum, G.B. Ellison, **Photoelectron spectroscopy, gas phase acidity, and thermochemistry of *tert*-butyl hydroperoxide: Mechanisms for the rearrangement of peroxyl radicals**, J. Chem. Phys. 109 (1998) 10293.

[42] I.R. Slagle, Q. Feng, D. Gutman, **Kinetics of the reaction of ethyl radicals with molecular oxygen from 294 to 1002 K**, J. Phys. Chem. 88 (1984) 3648-3653.

[43] A.F. Wagner, I.R. Slagle, D. Sarzynski, D. Gutman, **Experimental and theoretical studies of the ethyl + oxygen reaction kinetics**, J. Phys. Chem. 94 (1990) 1853-1868.

[44] J.A. Howard, K.U. Ingold, **Self-reaction of *sec*-butylperoxy radicals. Confirmation of the Russell mechanism**, J. Am. Chem. Soc. 90 (1968) 1056-1058.

[45] J.A. Howard, J.C. Scaiano, **Oxyl, peroxyl and related radicals, in: H Fischer (Ed.), Landolt-Börnstein numerical data and functional relations in science and technology**, new series, vol. 13, Springer-Verlag, New York, 1984.

[46] L. Jun-Na, C. Zhi-Rang, Y.J. Shen-Fang, **Study on the prediction of visible absorption maxima of azobenzene compounds**, Zhejiang Univ. Sci. B 6 (2005) 584-589.

Graphical abstract

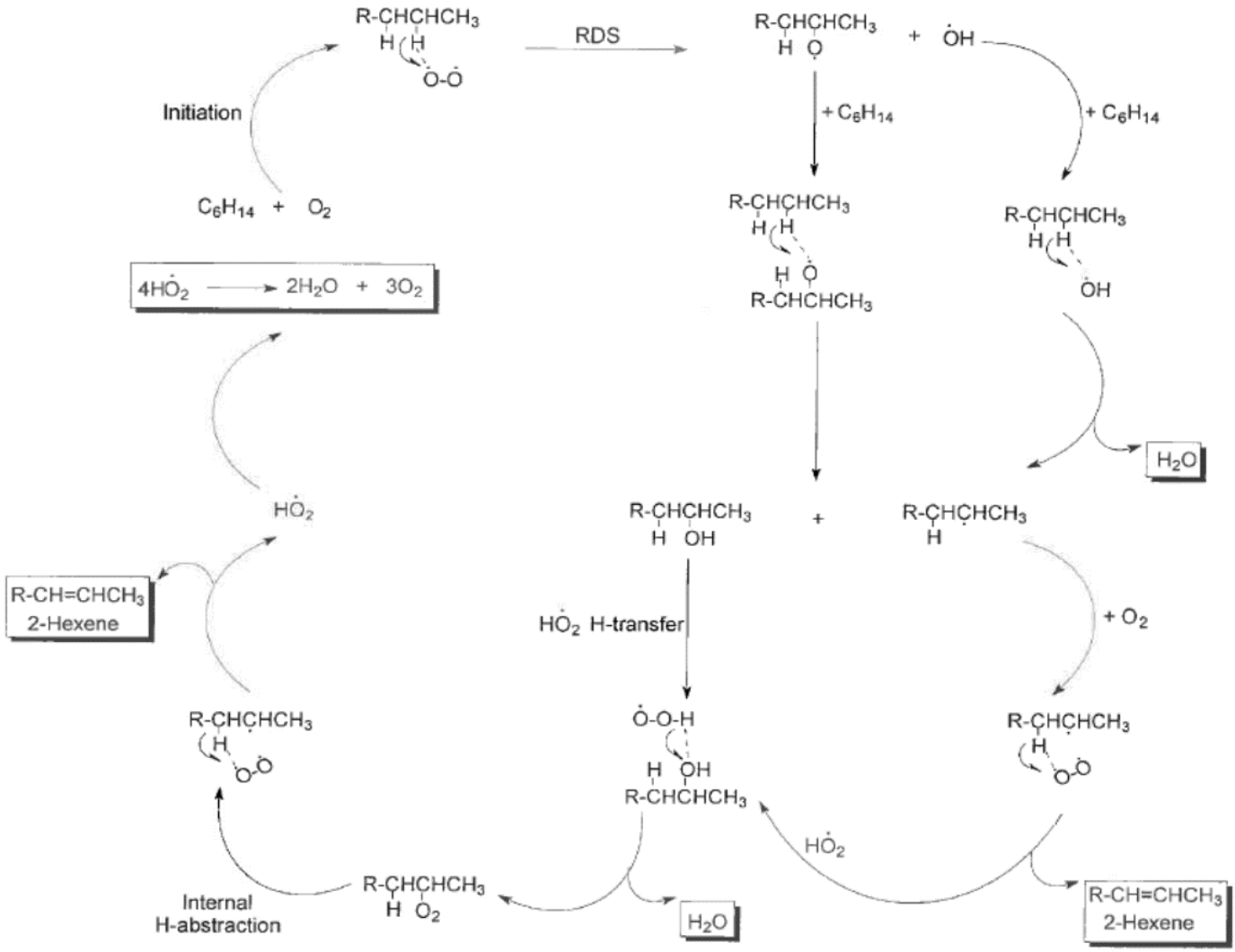

Figure 1 Proposed reaction scheme, with R=$CH_2CH_2CH_3$.

Highlights

- Activation step is H-abstraction from C_6H_{14} by O_2 to form $C_6H_{13}O\cdot$ and $\cdot OH$ radicals.
- $C_6H_{13}O\cdot$ and $\cdot OH$ radicals activate further C_6H_{14} molecules to produce $C_6H_{13}OH$ and H_2O.
- Also produced is $\cdot C_6H_{13}$ that forms 2-hexene and $HOO\cdot$ via H-abstraction by O_2.
- Hydrogen transfer from $HOO\cdot$ to $C_6H_{13}OH$ leads to H_2O and $C_6H_{13}OO\cdot$.
- $C_6H_{13}OO\cdot$ undergoes intramolecular H-abstraction to yield 2-hexene and $HOO\cdot$ radical.